A Comparison of Snow Depth on Sea Ice Retrievals Using Airborne Altimeters and an AMSR-E Simulator

Donald J. Cavalieri, Thorsten Markus, Alvaro Ivanoff, Jeff A. Miller, Ludovic Brucker, M. Sturm, James A. Maslanik, John F. Heinrichs, Albin J. Gasiewski, *Fellow, IEEE*, Carl Leuschen, William Krabill, and J. Sonntag

Abstract*—A comparison of snow depths on sea ice was made using airborne altimeters and an Advanced Microwave Scanning Radiometer for the Earth Observing System (AMSR-E) simulator. The data were collected during the March 2006 National Aeronautics and Space Administration (NASA) Arctic field campaign utilizing the NASA P-3B aircraft. The campaign consisted of an initial series of coordinated surface and aircraft measurements over Elson Lagoon, Alaska and adjacent seas followed by a series of large-scale (100 km × 50 km) coordinated aircraft and AMSR-E snow depth measurements over portions of the Chukchi and Beaufort seas. This paper focuses on the latter part of the campaign. The P-3B aircraft carried the University of Colorado Polarimetric Scanning Radiometer (PSR-A), the NASA Wallops Airborne Topographic Mapper (ATM) lidar altimeter, and the University of Kansas Delay-Doppler (D2P) radar altimeter. The PSR-A was used as an AMSR-E simulator, whereas the ATM and D2P altimeters were used in combination to provide an independent estimate of snow depth. Results of a comparison between the altimeter-derived snow depths and the equivalent AMSR-E snow depths using PSR-A brightness temperatures calibrated relative to AMSR-E are presented. Data collected over a frozen coastal polynya were used to intercalibrate the ATM and D2P altimeters before estimating an altimeter snow depth. Results show that the mean difference between the PSR and altimeter snow depths is −2.4 cm (PSR minus altimeter) with a standard deviation of 7.7 cm. The RMS difference is 8.0 cm. The overall correlation between the two snow depth data sets is 0.59.

***Index Terms*—Author, please supply index terms/keywords for your paper. To download the IEEE Taxonomy go to http://www.ieee.org/documents/2009Taxonomy_v101.pdf.** AQ1

Manuscript received May 31, 2011; revised October 20, 2011; accepted November 25, 2011.

D. J. Cavalieri is with D J Cavalieri, Sandy Spring, MD 20860 USA, and also with NASA Goddard Space Flight Center, Cryospheric Sciences Laboratory, Greenbelt, MD 20771 USA (e-mail: Donald.J.Cavalieri@nasa.gov).

T. Markus is with NASA Goddard Space Flight Center, Cryospheric Sciences Laboratory, Greenbelt, MD 20771 USA (e-mail: thorsten.markus@nasa.gov).

A. Ivanoff is with NASA Goddard Space Flight Center, Cryospheric Sciences Laboratory, Greenbelt, MD 20771 USA, and also with ADNET Systems, Inc. Rockville, MD 20852 USA (e-mail: Alvaro.Ivanoff@nasa.gov).

J. A. Miller is with NASA Goddard Space Flight Center, Cryospheric Sciences Laboratory, Greenbelt, MD 20771 USA, and also with Wyle Information Sciences, McLean, VA 22102 USA (e-mail: jeff.miller@nasa.gov).

L. Brucker is with NASA Goddard Space Flight Center, Cryospheric Sciences Laboratory, Greenbelt, MD 20771 USA, and also with Universities Space Research Association, Goddard Earth Sciences Technology and Research Studies and Investigations, Columbia, MD 21044-3432 USA (e-mail: ludovic.brucker@nasa.gov).

M. Sturm is with U.S. Army Cold Regions Research and Engineering Laboratory, Fort Wainwright, AK 99703 USA (e-mail: matthew.sturm@usace.army.mil).

J. A. Maslanik is with Colorado Center for Astrodynamics Research, University of Colorado, Boulder, CO 80262 USA (e-mail: james.maslanik@colorado.edu).

J. F. Heinrichs is with the Department of Geosciences, Fort Hays State University, Hays, KS 67601 USA (e-mail: jheinric@fhsu.edu).

A. J. Gasiewski is with the Department of Electrical and Computer Engineering, University of Colorado, Boulder, CO 80309 USA (e-mail: al.gasiewski@colorado.edu).

C. Leuschen is with Center for the Remote Sensing of Ice Sheets, University of Kansas, Lawrence, KS 66045 USA (e-mail: leuschen@cresis.ku.edu).

W. Krabill is with NASA Goddard Space Flight Center, Cryospheric Sciences Laboratory, Greenbelt, MD 20771 USA, and also with Sigma Space, Inc., Wallops Island, VA 23337 USA (e-mail: William.B.Krabill@nasa.gov).

J. Sonntag is with EG&G Technical Services, NASA Goddard Space Flight Center, Greenbelt, MD 20771 USA (e-mail: john.g.sonntag@nasa.gov).

Color versions of one or more of the figures in this paper are available online at http://ieeexplore.ieee.org.

Digital Object Identifier 10.1109/TGRS.2011.2180535

I. Introduction

The PRIMARY objective of the National Aeronautics and Space Administration (NASA) March 2006 Arctic field campaign was to assess the accuracy of the Aqua Advanced Microwave Scanning Radiometer for the Earth Observing System (EOS) (AMSR-E) snow depth on sea ice retrievals [1]. The field campaign consisted of an initial series of coordinated surface and NASA P-3B aircraft measurements over Elson Lagoon, Alaska and adjacent seas on March 18 and 20 followed by a series of large-scale (100 km × 50 km) coordinated aircraft and Aqua AMSR-E measurements over portions of the Chukchi Sea, Kotzebue Sound, and the Beaufort Sea on March 21, 22, and 25, respectively. A sixth flight on March 24 was coordinated with an ICESat overpass in the high Arctic to support a study of the effects of snow cover variability on ice thickness retrievals from the ICESat laser altimeter [2]. All six flights were made from Fairbanks International Airport, Alaska [Fig. 1(a)]. A transit flight to Greenland was also made on March 27 in coordination with an Envisat Radar Altimeter-2 overpass in the high Arctic to validate sea ice elevation measurements derived from the Envisat microwave altimeter [3].

The Elson Lagoon flights on March 18 and 20 were used to compare in-situ snow depth measurements with snow depth measurements made from the airborne radiometer and altimeters. The results from these flights will be the subject of a forthcoming paper. In this paper, we use data collected over the flight areas of March 21, 22, and 25 [Fig. 1(a)] to compare

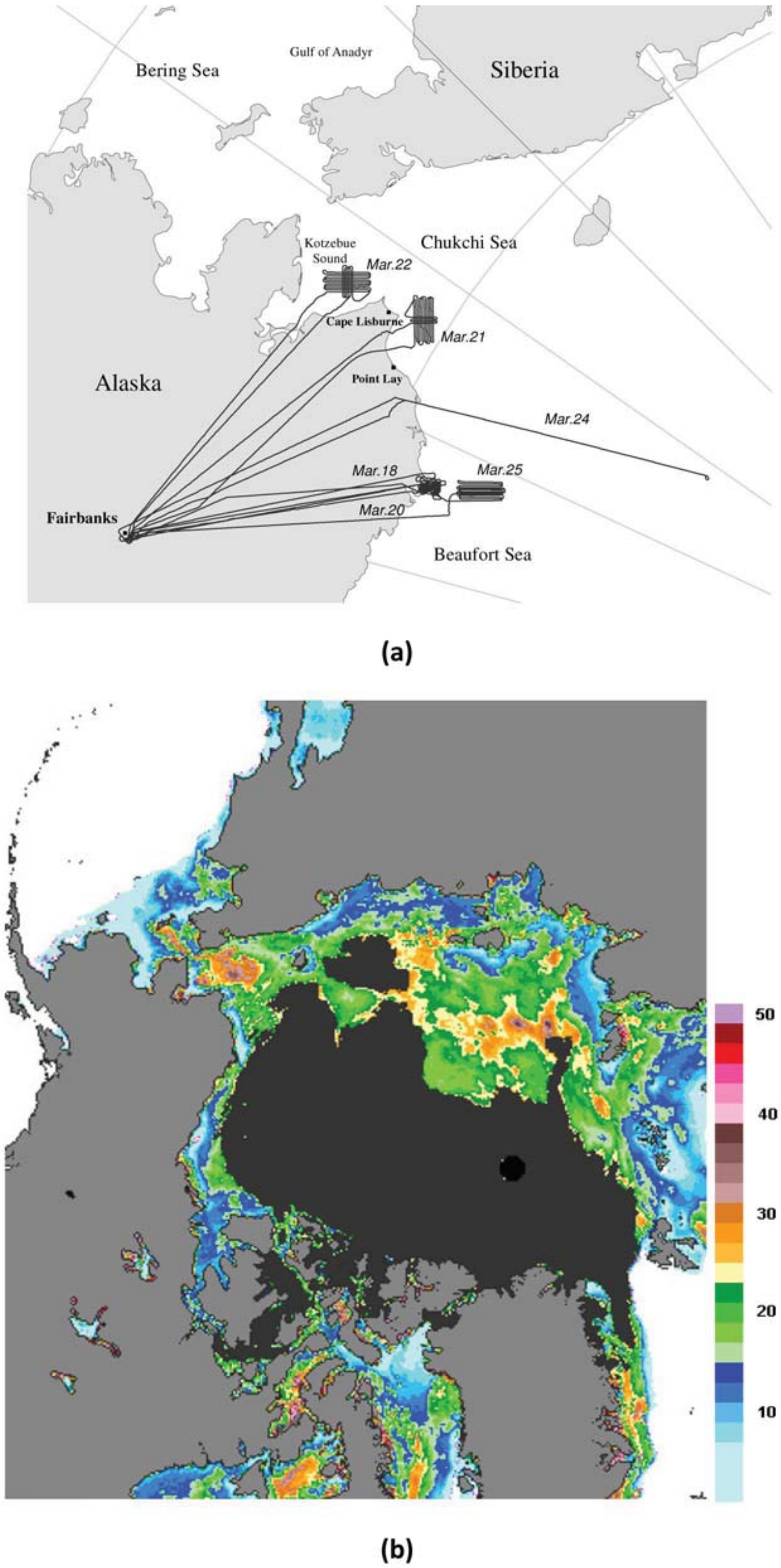

Fig. 1. (a) Six NASA P-3B flights made from Fairbanks, AK covered portions of Elson Lagoon near Pt. Barrow, AK, the Chucki and Beaufort seas, Kotzebue Sound, and the high Arctic during the March 2006 AMSR-E Arctic field campaign. (b) AMSR-E snow depth map (5-day average) for March 21, 2006. The color scale gives the snow depth in centimeters. Multiyear sea ice is masked out, because the snow depth retrievals are limited to first-year sea ice types only. 4/C

the snow depth retrievals obtained from the NASA P-3B altimeters and from the radiometer which has the same radiometric channels as the AMSR-E sensor. Even with the aircraft making two or three passes over an AMSR-E 12.5 km grid cell, the coverage by the aircraft sensors was too sparse for a direct comparison with AMSR-E snow depths. Thus, we use the airborne radiometer as an AMSR-E simulator to compare the microwave radiometer and altimeter snow depths. Previous work used

TABLE I
NASA P-3B AIRCRAFT SENSORS FLOWN DURING THE ARCTIC 2006 FIELD CAMPAIGN

Sensor	Characteristics	FOV at 680 ft Altitude	Estimated Precision	Purpose
Polarimetric Scanning Radiometer (PSR-A and PSR-CX)	Operating Frequencies (H&V-pol):6, 10, 18, 22, 37, 89 GHz	67 m	1-2 K	Aircraft AMSR-E simulator microwave based snow depth determination
Airborne Topographic Mapper (ATM-II)	Scanning Lidar altimeter combined with a differential GPS system	2 m (100m swath width)	10 cm [13]	Air/snow interface elevation, Maps ice surface topography at high resolution
Dual-Doppler Radar (Ku-band)	Delay-Doppler Phase-monopulse (D2P) radar altimeter data	30 m (across) x 4 m (along)	5 cm [12]	Sea ice/snow interface elevation
Digital Cameras	2 KODAK Digital cameras (3 megapixel)	170 m (across) x 260 m (along)		Visible record of ice surface

both the high-resolution airborne laser altimeter retrievals of snow-ice freeboard and the passive microwave retrievals of snow depth from this campaign to provide insight into the spatial variability of these quantities as well as optimal methods for combining high-resolution satellite altimeter measurements with low-resolution snow depth data [4].

The original intent of this work was to use the airborne altimeters as a validation tool to assess the AMSR-E sea snow on sea ice retrievals, but since the altimeter elevation differences used as a measure of snow depth on sea ice have yet to be validated, we present a comparison between the airborne altimeter-derived snow depths and the airborne microwave radiometer-derived snow depths using an equivalent AMSR-E snow depth on sea ice algorithm. The comparative results provide insight into the limitations of both the altimetric and radiometric snow depth retrievals.

II. METHODOLOGY

A. EOS Aqua AMSR-E Satellite Data

The AMSR-E was launched in May 2002 on the Aqua satellite. AMSR-E is a state-of-the-art sensor measuring microwave emissions over a broader range of wavelengths and with better spatial resolution than previous satellite radiometers. AMSR-E was designed and built by the Japan Aerospace Exploration Agency for the NASA EOS Aqua spacecraft [5]. The three AMSR-E sea ice products include sea ice concentration, snow depth on sea ice, and sea ice drift. In this paper, we make use of the snow depth on sea ice product.

AMSR-E snow depth on sea ice is a 5-day averaged gridded product at a resolution of 12.5 km and is derived using an algorithm described by [6]. While the product is available for both the Antarctic and Arctic, in the latter region, the snow depth retrievals are limited to areas of first-year sea ice, because multiyear ice presents a fundamental ambiguity, which is discussed later, making the retrieval of snow depth over multiyear ice indeterminate, at least at present. An example of the 5-day AMSR-E snow depth product is shown in Fig. 1(b).

As described in [6], the snow depth on sea ice algorithm is linearly related to the spectral gradient ratio corrected for sea ice concentration GRV (ice) defined by

$$\mathrm{GRV(ice)} = [T_{\mathrm{b}}(37\mathrm{V}) - T_{\mathrm{b}}(18\mathrm{V}) - k_1(1-\mathrm{C})] \,/\, [T_{\mathrm{b}}(37\mathrm{V}) + T_{\mathrm{b}}(18\mathrm{V}) - k_2(1-\mathrm{C})] \quad (1)$$

where $T_{\mathrm{b}}(37\mathrm{V})$ and $T_{\mathrm{b}}(18\mathrm{V})$ are the brightness temperatures of the satellite radiometer and

$$k_1 = T_{\mathrm{bow}}(37\mathrm{V}) - T_{\mathrm{bow}}(18\mathrm{V}) \quad (2)$$

$$k_2 = T_{\mathrm{bow}}(37\mathrm{V}) + T_{\mathrm{bow}}(18\mathrm{V}). \quad (3)$$

T_{bow} is the open water brightness temperature, and C is the sea ice concentration as determined by the enhanced NASA Team (NT2) algorithm applied to the AMSR-E data [7].

The snow depth h_{s} in centimeters is given by

$$h_{\mathrm{s}} = a_1 + a_2\,\mathrm{GRV(ice)}. \quad (4)$$

Both the a_1 and a_2 coefficients were derived from a linear regression of in-situ snow depth measurements on SSM/I microwave measurements [6]. These coefficients were subsequently adjusted to take into account brightness temperature calibration differences between SSM/I and AMSR-E. For SSM/I equivalent GRV, a_1 has the value of 2.9 cm, and a_2 has the value of -782 cm.

The basis of the algorithm assumes that scattering increases with increasing snow depth and that the scattering efficiency is greater at 37 GHz than at 18 GHz. For snow-free first-year sea ice, the gradient ratio is close to zero, and it becomes more and more negative as the differential scattering increases resulting from an increase in snow depth and/or an increase in grain size. The upper limit for snow depth retrievals is about 50 cm which is a result of the limited penetration depth at 37 GHz [8].

The algorithm is applicable to dry snow conditions only. At the onset of melt, the emissivities of both the 18 GHz and the 37 GHz channels approach unity (that of a blackbody) and the gradient ratio approaches zero initially before becoming positive. Thus, snow depth is indeterminate under wet snow conditions. Snow, which can be wet during the day, frequently refreezes during the night. This refreezing results in very large grain sizes, which results in a reduced emissivity at 37 GHz relative to 18 GHz, thereby decreasing GRV (ice) and thus results in an overestimate of snow depth. These thaw-freeze events cause large temporal variations in the snow depth retrievals. This temporal information is used in the algorithm to flag the snow depths as indeterminate from those periods with large fluctuations. As in-situ grain size measurements are even less frequently collected than snow depth measurements, the influence of grain size variations could not be incorporated into the algorithm. Because of diurnal melt-freeze cycles and sporadic weather effects, AMSR-E daily snow depth products are 5-day running averages.

Because of the higher sensitivity of snow depth retrievals to ice concentrations less than 20%, the algorithm limits snow depth retrievals to ice concentrations between 20% and 100%. Ice concentrations less than 20% appear almost exclusively near the ice edge, so the total area excluded is relatively small.

Both multiyear ice and deep snow on top of first-year ice result in increasingly negative values for the spectral GR [9]; therefore, the algorithm only retrieves snow depth in the seasonal sea ice zones. We currently use a dynamic GRV based filter which approximates the multiyear sea ice cover. This multiyear ice mask is defined on October 1 of each year as sea ice which has GRV values of less than -0.03. The same GRV test is done for each subsequent day, with the resulting classification being limited by the boundary of the previous day's mask, with an allowance of a 1 pixel perimeter, to take into account the possible motion of the multiyear ice pack.

B. Aircraft Data Sets

The NASA P-3B aircraft carried the University of Colorado Polarimetric Scanning Radiometer (PSR-A), the NASA Wallops Airborne Topographic Mapper (ATM) lidar altimeter, and the University of Kansas Delay-Doppler (D2P) radar altimeter. The PSR-A was used as an AMSR-E simulator, whereas the ATM measured the range from the aircraft to the air/snow interface and the D2P measured the range from the aircraft to the sea ice/snow interface. The processing of the altimeter measured ranges is quite complex and is discussed in detail elsewhere (e.g., [10]–[12]). The altimeter products used in this study are given as elevations measured in meters relative to a common geoid. The difference in altimeter elevations (ATM-D2P) was used to provide an independent estimate of snow depth. A summary of the aircraft instrument operating characteristics as well as the estimated precision of the altimeters obtained from previous field campaigns is presented in Table I.

The method employed consisted of making three flights (March 21, 22, and 25) over large areas (100 km × 50 km) covering 32 AMSR-E grid elements (12.5 km on a side) on each day. The day before each of these flights, we utilized near real-time AMSR-E snow depth maps to plan the next day's flight. On March 21, we covered an area in the Chukchi Sea which had a relatively shallow snow cover [Fig. 2(a)]. On March 22, we overflew an area in Kotzebue Sound which had a somewhat deeper snow cover [Fig. 2(b)], and on March 25, we flew over an area in the Beaufort Sea which had the largest apparent snow cover [Fig. 2(c)]. The orientation of each rectangular box in Fig. 2 matches the orientation of the flight lines shown in Fig. 1(a) for corresponding days.

For the purpose of utilizing the PSR as an AMSR-E simulator, we calibrated the PSR 19 GHz V-pol. and 37 GHz V-pol. brightness temperatures relative to AMSR-E making use of all the data obtained for March 21, 22, and 25 resulting in a total of 96 data points (Fig. 3). The justification for using the PSR as a proxy for AMSR-E is the high correlation (0.94) between the AMSR-E and PSR GRV parameters (Fig. 4).

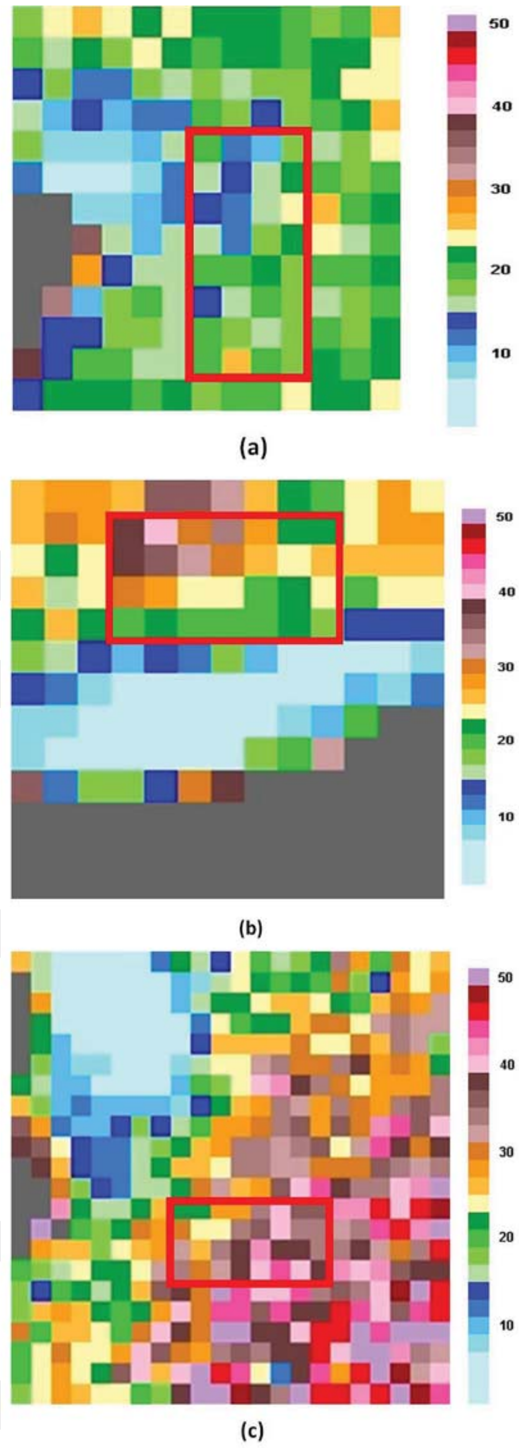

Fig. 2. AMSR-E snow depths for portions of (a) the Chukchi Sea overflown on March 21, (b) Kotzebue Sound overflown on March 22, and (c) the Beaufort Sea overflown on March 25. The red rectangle in each image indicates the approximate area overflown by the NASA P-3B aircraft. Each rectangle measures 4 by 8 12.5 km AMSR-E pixels. The color scale gives snow depths in cm. 4/C

Once the PSR 19V and 37V brightness temperatures were converted to equivalent AMSR-E brightness temperatures using the regression equations shown in Fig. 3, the AMSR-E snow depth algorithm was applied [(1) and (4)] to obtain PSR snow depths.

Field airborne laser and radar altimeter measurements show that the difference between the ATM elevation and the D2P

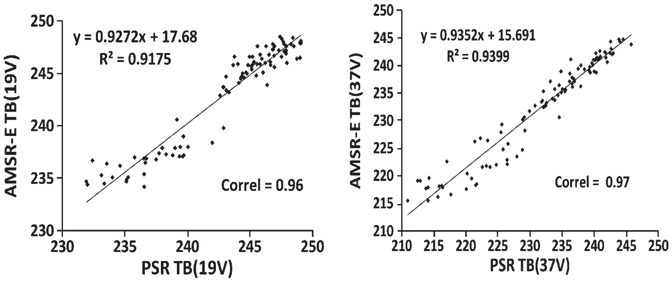

Fig. 3. AMSR-E versus PSR regression plot for TB(19V) (left) and TB(37V) (right).

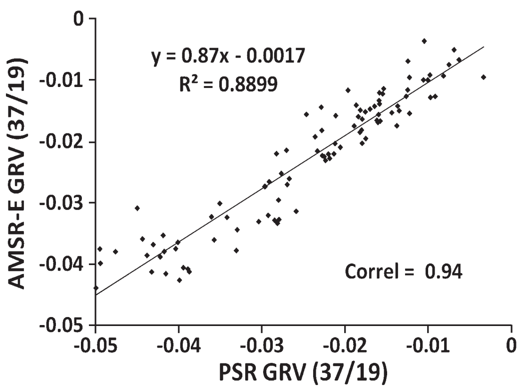

Fig. 4. AMSR-E versus PSR GRV regression plot.

elevation provides a snow depth estimate consistent with climatologies [14], because the ATM measures the elevation of the air/snow interface and the D2P measures the elevation of the snow/ice interface both relative to a common geoid. Before using the altimeters as an alternate means of providing estimated snow depths, we needed to calibrate them relative to each other over some sea ice surface with a known snow depth. Newly frozen leads or polynyas provide such a surface. The rationale is that the ATM and D2P elevations should match over newly formed ice because there is only a minimal snow cover, if any at all. An analysis of ATM and D2P elevations measured over frozen leads and polynyas on all three days showed that the area with a minimum ATM-D2P elevation variance (2.41 cm) occurred over the frozen coastal polynya on March 22. The mean difference was -9.93 cm indicating that we needed a 10 cm offset in the D2P elevations to obtain agreement between the two altimeters. While we cannot be sure that there was no snow cover, without this offset there were 122 negative snow depths obtained with a maximum negative value of -12 cm, whereas with the offset there were only 17 negative values the largest being -2 cm.

Fig. 5 shows an Aqua MODIS image with the NASA P-3 flight tracks superimposed for March 22, 2006. Segment A of the flight track over the coastal polynya was used to intercalibrate the two altimeters. The three aerial photographs shown as insets in Fig. 5 confirm that this segment was comprised of newly formed sea ice. Fig. 6 shows the effect of the 10-cm offset as applied to the D2P elevations which brings the ATM and D2P elevations into better agreement over frozen leads in a portion of the March 22 flight (segment B on Fig. 5).

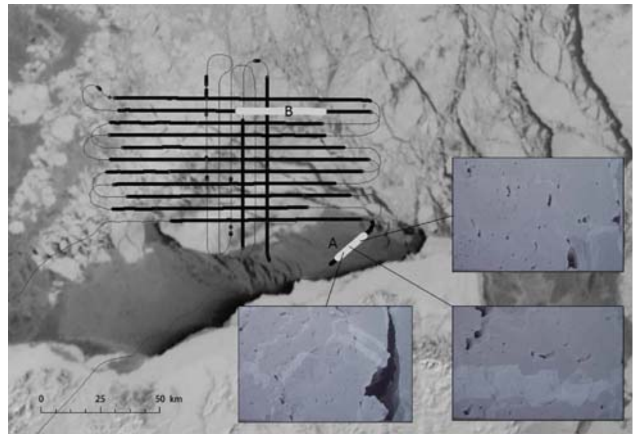

Fig. 5. NASA P-3 flight tracks (gray thin lines) on an Aqua MODIS image of Kotzebue Sound for March 22. The aircraft altimeter data coverage is also shown (black heavy lines). The segment highlighted within the large area of grey ice (segment A) off the Alaskan coast was used to determine the altimeter elevation statistics and the resulting offset between the ATM and D2P elevations. The inset images are captured from the onboard digital camera and show the character of the ice surface within the coastal polynya. Segment B is the portion of the flight track used for the profiles in Fig. 6.

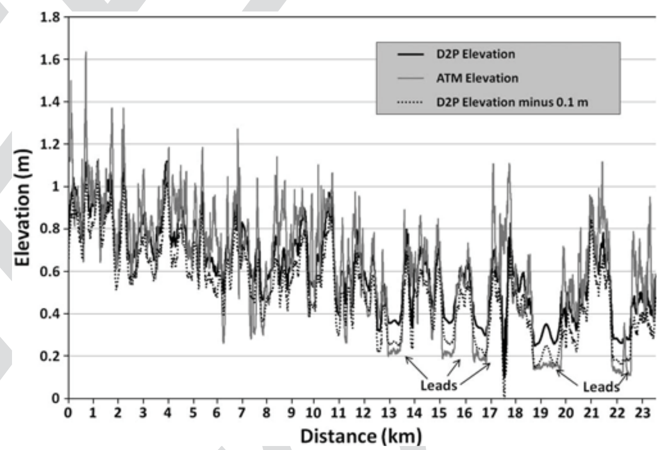

Fig. 6. Portion of the March 22 flight (segment B on Fig. 5) shows that a 10-cm offset applied to the D2P elevations brings the ATM and D2P elevations into better agreement over frozen leads.

Finally, for the purpose of obtaining a geolocated airborne sensor data set, the D2P altimeter data were chosen as the reference location. The ATM elevation and PSR brightness temperature data were averaged over a 35 m diameter circle around each given valid D2P point. The 35-m data sets were smoothed either to a 1-km length scale or to the 12.5-km AMSR-E grid scale for the comparison studies discussed below.

III. Results and Discussion

The sea ice and snow cover characteristics of the areas overflown on March 21, 22, and 25 are all quite different and are discussed in the context of their microwave polarization (PR) and spectral gradient (GR) signatures. PR is defined in terms of the 19-GHz horizontal and vertical polarization PSR channels

$$\mathrm{PR19} = [\mathrm{TB19V} - \mathrm{TB19H}]/[\mathrm{TB19V} + \mathrm{TB19H}]. \quad (5)$$

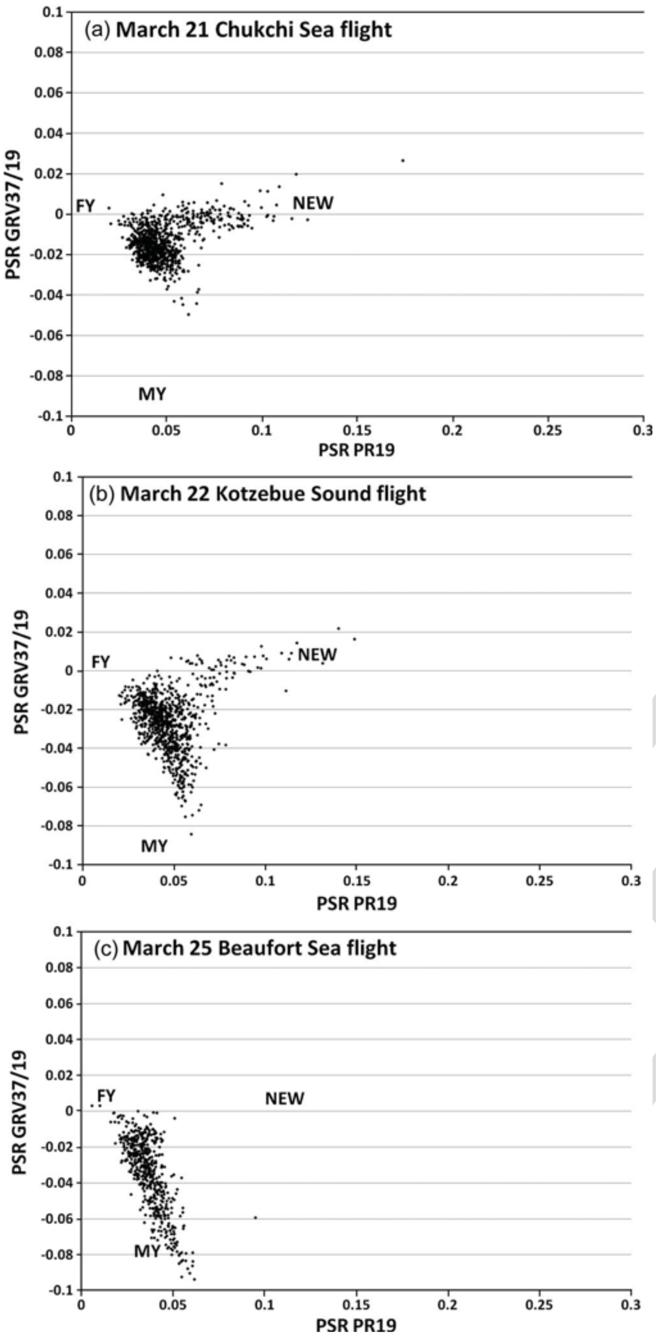

Fig. 7. Plots illustrate the differences in PSR microwave PR-GR signatures for the three study areas on (a) March 21, (b) March 22, and (c) March 25, 2006. In each plot, the locations of pure first-year (FY), new (NEW), and multiyear (MY) ice types are indicated.

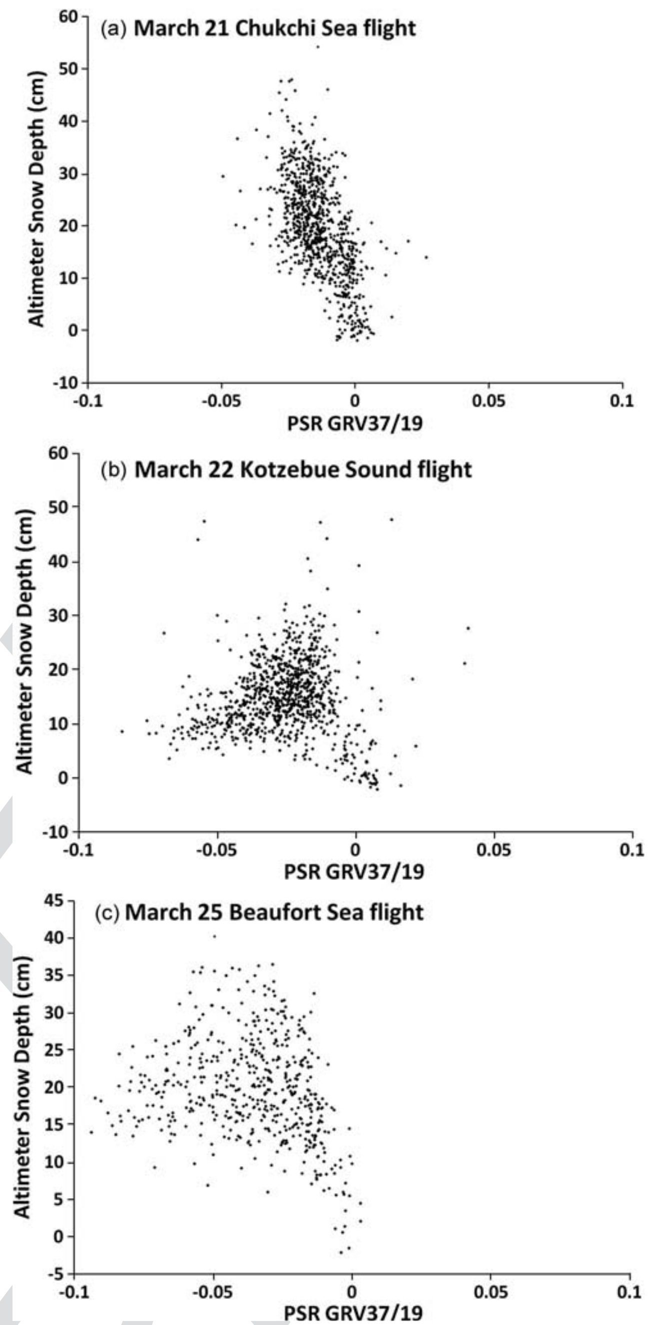

Fig. 8. Plots illustrate the relationship between the altimeter measured snow depths and the PSR GRV signatures for the three study areas on (a) March 21, (b) March 22, and (c) March 25, 2006.

Whereas GR is defined in terms of the 19-GHz and 37-GHz vertical polarization PSR channels

$$\mathrm{GRV37/19} = [\mathrm{TB37V} - \mathrm{TB19V}/[\mathrm{TB37V} + \mathrm{TB19V}]. \quad (6)$$

The PR-GR characteristics of each of these three areas are shown in Fig. 7 through the use of PR-GR scatter plots. The PR-GR plot for March 21 [Fig. 7(a)] shows a fairly tight cluster near PR of 0.05 and GRV of -0.02 which is typical of first-year ice types (e.g., [9]; [15]). A looser cluster of points, typical of new and young ice types, straddles the GRV value of 0 and extends to higher PR values. The plot for March 22 [Fig. 7(b)] shows that in addition to the typical first-year ice distribution of points, many points have more negative GRV values. The more negative GRV values are likely the result of deeper snow and the effects of the melt/freeze event that occurred in mid February which may have resulted in a snow cover with ice layers resulting in more scattering of the 37-GHz radiation relative to 19 GHz. Finally, the area overflown on March 25 was comprised of first-year and multiyear sea ice with no new and young ice types [Fig. 7(c)].

Scatter plots of the altimeter snow depths versus the PSR GRV values for each of the three study areas overflown are shown in Fig. 8. The expected linear relationship between the

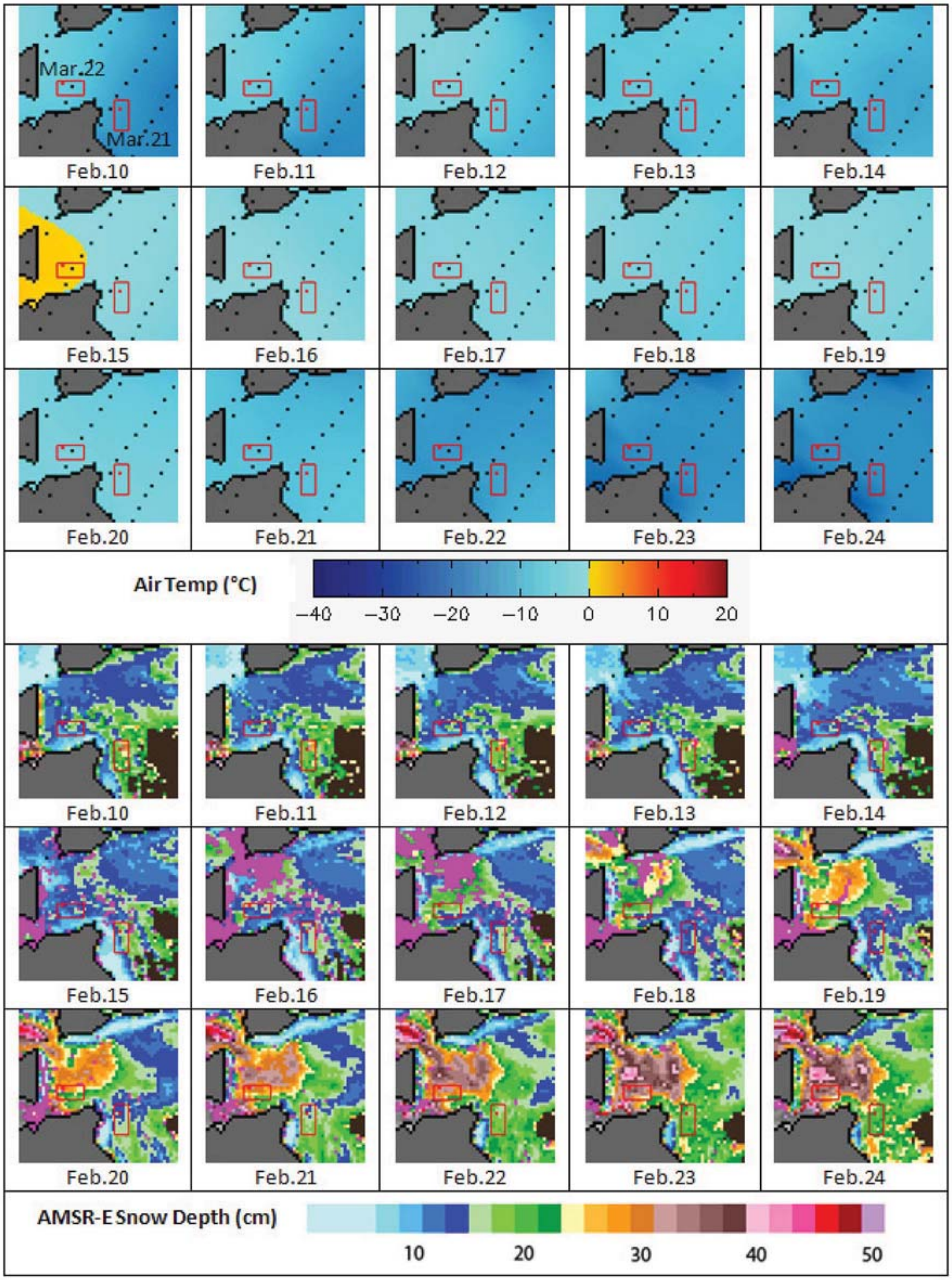

Fig. 9. Sequence of images showing daily-averaged ECMWF surface atmospheric temperatures (top) and AMSR-E snow depth retrievals (bottom) for a two-week period in February 2006. The study areas overflown on March 21 and 22 are indicated by red rectangles. 4/C

microwave parameter GRV, which is the independent variable in the snow depth algorithm [6], and the altimeter snow depth is lost for the March 22 and March 25 areas. Only for the March 21 area does the linear relationship hold [Fig. 8(a)].

Reasons for the lack of correlation for March 22 and 25 [Fig. 8(b) and (c)] are difficult to determine with certainty. The lack of correlation for the March 25 flight in the Beaufort Sea is probably related to the large fraction of multiyear ice in the region. However, the March 22 area in Kotzebue Sound is devoid of multiyear ice, but contains ice having more negative GRV values [Fig. 7(b)] than is normally observed in first-year ice regions. As noted earlier, there was a large-scale melt-freeze event in Kotzebue Sound during mid-February 2006. Fig. 9 shows a sequence of daily ECMWF (ERA-interim) atmospheric

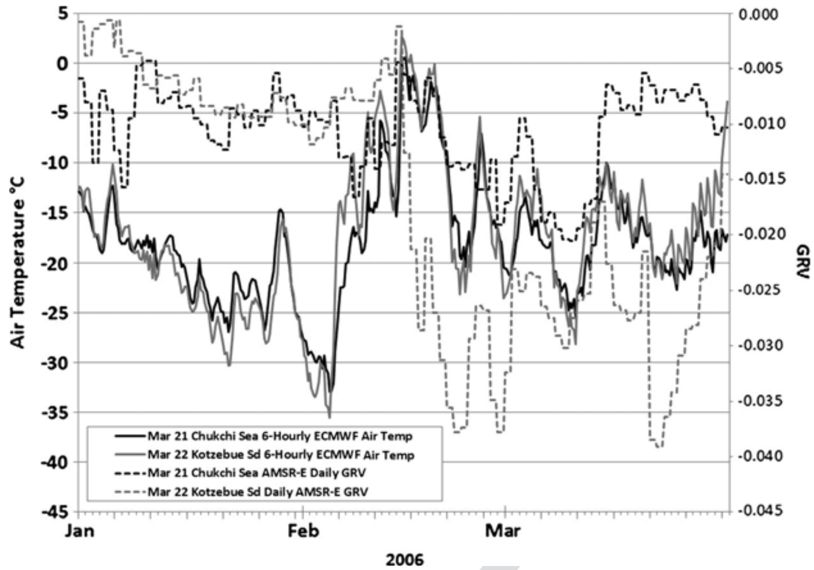

Fig. 10. Time series of the first 90 days of 2006 showing 6-hourly ECMWF surface air temperatures and daily AMSR-E GRV values corresponding to the highlighted pixels in Fig. 9 for March 21 and 22. February 15, 2006 is the day when the air temperature exceeded 0 C. Note the difference in the behavior of the AMSR-E GRV values for the two flight regions after the onset of melt.

temperatures and AMSR-E snow depth maps during mid-February covering both the Chukchi Sea and Kotzebue Sound flight areas overflown on March 21 and 22, respectively. It is clear from Fig. 9 that the flight area over Kotzebue Sound had positive daily-averaged air temperatures in mid-February, whereas the flight area over the Chukchi Sea had not. In particular, during the period from February 14–20, two low pressure systems initially centered over the Gulf of Anadyr [Fig. 1(a)] migrated into the Chukchi and Beaufort seas, resulting in a combination of southerly winds, increased air temperatures, and a likely increase in down-welling, long-wave radiation associated with increased cloud cover. With air temperatures near zero, it is also possible that some precipitation may have fallen as rain, which would have significantly affected the scattering properties of the snow cover. The Kotzebue weather station reported warming daily air temperatures from the beginning of February to February 15 when the maximum temperature of 1.1°C was reached. An increase in snow on the ground was not reported until February 25 when the measured snow and ice on the ground doubled to 28 cm. The maximum snow cover of 43 cm reported at Kotzebue was reached during mid-March. The weather conditions and melt event in Kotzebue Sound may have resulted in a combination of deep snow and a metamorphosed snow cover with ice layers and coarser-grained snow. This melt event which affected the entire flight area is a probable cause for the lack of correlation shown in Fig. 8(b).

Fig. 10 provides a time series of 6-hourly ECMWF surface air temperatures [16] and daily AMSR-E GRV values for the highlighted (red) pixels shown in Fig. 9 for the first three months of 2006. The red pixel within the red rectangle for Kotzebue Sound is located in the upper left portion of the flight area, and the red pixel for the Chukchi Sea is in the upper portion (Fig. 9). Following February 15, 2006, the day of maximum air temperature (+1.08 C), there is a marked difference in the behavior of the AMSR-E GRV values for the two flight regions after the onset of melt. The Chukchi Sea region apparently did not undergo the same degree of surface melt on February 15 (Fig. 10). In fact, none of the 32 grid cells overflown on March 21 had daily average air temperatures above −0.9 C with the warmest temperatures occurring closest to Kotzebue Sound [upper left in Fig. 2(a)]. The average of the daily air temperatures on February 15 for the 32 grid cells overflown on March 21 was −1.4 C. The GRV values for both regions decreased initially after the melt event. The Chukchi Sea GRV values became less negative beginning on March 12 and maintained values between −0.005 and −0.01 from March 14 through March 29 (Fig. 10). The GRV values in this range are typical of new, young, and thin first-year ice types. Because the Chukchi Sea region is much more dynamic than Kotzebue Sound, one possibility is that the February Chukchi Sea ice cover was displaced by sea ice having different (younger) surface characteristics. To explore this possibility, we compare daily AMSR-E snow depth maps with IFREMER (Institut Français de Recherche pour l'exploitation de la Mer, Issy-les-Moulineaux, France) AMSR-E sea ice drift maps obtained from (ftp://ftp.ifremer.fr/ifremer/cersat/products/gridded/psi-drift/documentation/amsr.pdf) for a 10-day period in March 2006. These maps are shown in Fig. 11.

From March 13 through March 17 the sea ice drift was toward the north, but from March 18, 19, and 20, there was even stronger ice drift away from the Alaskan coast (Fig. 11). The Alaskan coast region between Cape Lisburne and Point Lay [Fig. 1(a)] produces a large volume of ice each winter through oceanic heat loss by coastal polynyas. The ice produced is often swept up in large-scale cyclonic or anticyclonic gyres and transported to other parts of the Arctic Ocean. The snow depth maps in Fig. 11 show an increasingly large area of ice with a shallow snow cover. Presumably, recently formed new and young ice types were advected into the area overflown on March 21 resulting in less negative GRV values (Fig. 10).

Next, we examine the AMSR-E pixel-averaged D2P and ATM elevations, the altimeter and PSR snow depths, the

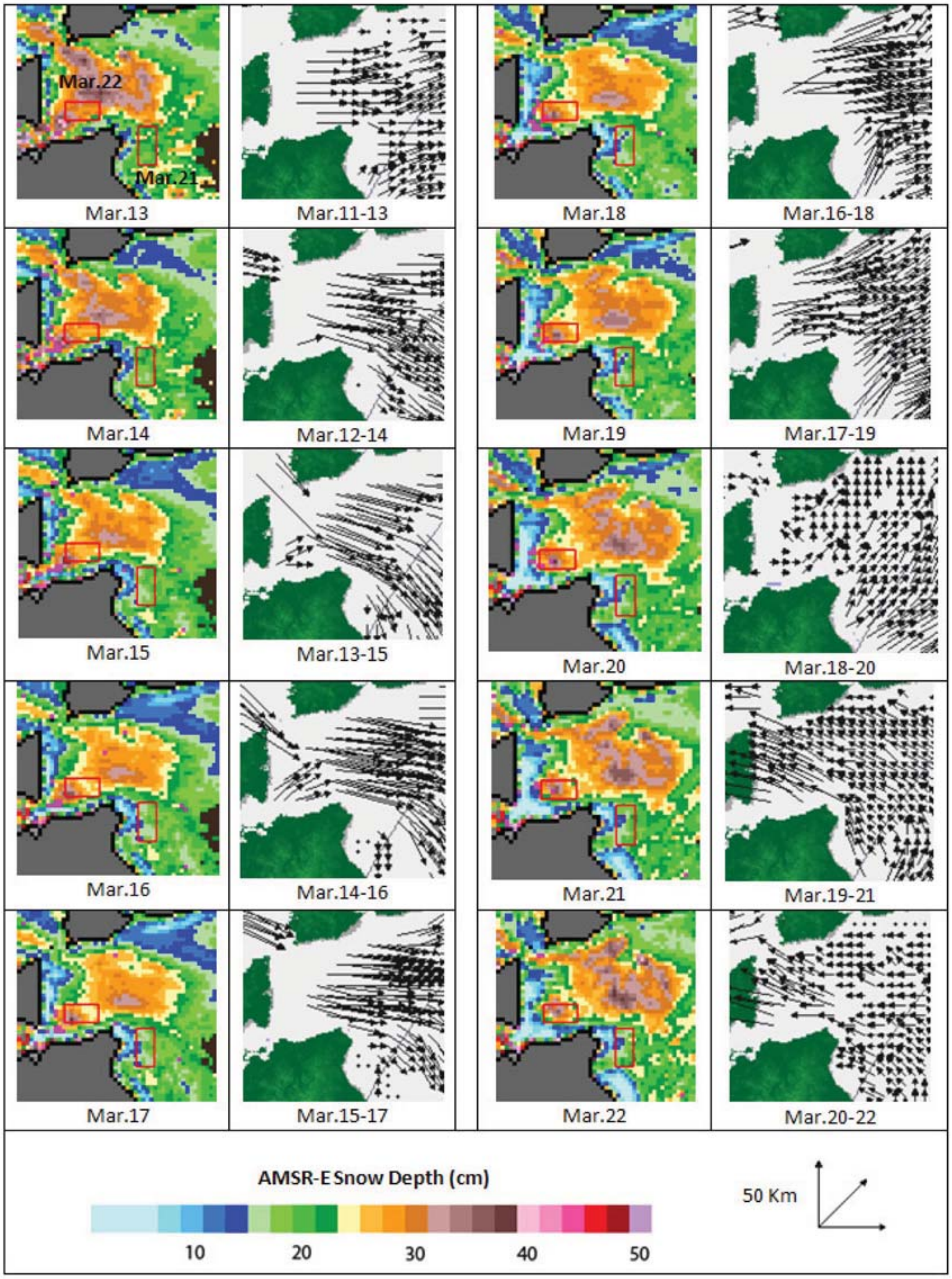

Fig. 11. Sequence of images showing IFREMER AMSR-E sea ice drifts for a 2-day period together with the AMSR-E snow depths from March 13 to March 22 in the vicinity of Kotzebue Sound and the Chukchi Sea. The overflight areas for the Chukchi Sea on March 21 and for Kotzebue Sound on March 22 are indicated by red rectangles as in Fig. 9. 4/C

ATM-derived surface roughness, and the AMSR-E snow depths for both the Chukchi Sea region overflown on March 21 (Table II) and the Kotzebue Sound region overflown on March 22 (Table III). The orientation of the AMSR-E grid elements in Table II is rotated 90° relative to the AMSR-E cells shown in Fig. 2(a). The orientation of the grid elements in Table III is similar to that shown in Fig. 2(b). The surface roughness was obtained by calculating the average standard deviation of the ATM elevations over each AMSR-E grid cell in each table.

In Table II, for the Chukchi Sea area, both the D2P and ATM elevations show similar spatial patterns as do the altimeter and PSR snow depths with the deepest snow found in the upper left and lower right portions of the 32-cell grid. A comparison of the ATM roughness values with the altimeter and PSR snow

TABLE II

MEAN (A) D2P ELEVATION, (B) ATM ELEVATION, (C) ALTIMETER SNOW DEPTH, (D) PSR SNOW DEPTH, (E) ATM ROUGHNESS, AND (F) AMSR-E SNOW DEPTH FOR EACH OF THE 32 AMSR-E GRID ELEMENTS (COLUMN, ROW) OVERFLOWN ON MARCH 21, 2006. SHADES OF GRAY FROM LIGHT TO DARK ARE USED TO INDICATE INCREASING VALUES FROM LOW TO HIGH. THERE WAS NO AIRCRAFT COVERAGE OF GRID (377,156)

A) D2P Elevation	370	371	372	373	374	375	376	377
154	0.6091	0.6550	0.4342	0.4272	0.4422	0.3525	0.3446	0.2287
155	0.4924	0.4986	0.5455	0.6505	0.4802	0.4817	0.4313	0.4196
156	0.4353	0.6096	0.7945	0.7141	0.6537	0.5595	0.5269	
157	0.4060	0.6141	0.7147	0.6279	0.6293	0.6689	0.5432	0.5194
B) ATM Elevation	370	371	372	373	374	375	376	377
154	0.9657	0.8950	0.5507	0.5879	0.6530	0.5395	0.5522	0.4453
155	0.6550	0.6419	0.7050	0.8923	0.6657	0.6488	0.6287	0.6806
156	0.6669	0.8326	1.0683	0.9583	0.8632	0.7195	0.7236	
157	0.5284	0.8244	0.9221	0.7715	0.7593	0.8433	0.7359	0.8126
C) Altimeter SD	370	371	372	373	374	375	376	377
154	35.66	24.00	11.65	16.07	21.09	18.70	20.76	21.66
155	16.25	14.33	15.95	24.17	18.54	16.72	19.73	26.09
156	23.15	22.30	27.39	24.43	20.95	16.00	19.67	
157	12.24	21.03	20.74	14.36	13.00	17.44	19.27	29.32
D) PSR SD	370	371	372	373	374	375	376	377
154	24.83	18.97	9.91	12.78	16.78	14.25	17.18	19.33
155	11.27	9.41	11.91	16.39	13.62	14.21	18.57	25.17
156	16.27	18.73	21.33	19.87	20.34	18.43	19.22	
157	11.99	20.70	22.67	16.98	15.19	17.94	19.01	26.27
E) ATM Roughness	370	371	372	373	374	375	376	377
154	21.86	22.21	9.71	16.68	18.60	18.18	19.53	17.27
155	17.08	14.70	16.38	25.15	17.81	18.08	18.19	23.89
156	19.21	22.71	25.09	24.27	21.07	15.58	18.00	
157	16.21	26.64	25.86	20.85	17.78	16.85	20.37	21.85
F) AMSR-E SD	370	371	372	373	374	375	376	377
154	19.40	16.86	13.42	14.28	16.24	16.91	19.00	19.42
155	16.40	13.76	12.73	15.07	17.56	15.73	20.01	25.71
156	14.72	17.57	19.27	18.39	19.20	18.51	17.08	
157	16.23	22.41	25.03	19.30	18.73	20.38	19.40	21.35

TABLE III

MEAN (A) D2P ELEVATION, (B) ATM ELEVATION, (C) ALTIMETER SNOW DEPTH, (D) PSR SNOW DEPTH, (E) ATM ROUGHNESS, AND (F) AMSR-E SNOW DEPTH FOR EACH OF THE 32 AMSR-E GRID ELEMENTS (COLUMN, ROW) OVERFLOWN ON MARCH 22, 2006. SHADES OF GRAY FROM LIGHT TO DARK ARE USED TO INDICATE INCREASING VALUES FROM LOW TO HIGH

A) D2P Elevation	136	137	138	139	140	141	142	143
364	1.810	1.664	1.436	1.071	0.704	0.454	0.306	0.300
365	1.773	1.552	1.209	0.850	0.566	0.361	0.281	0.240
366	1.719	1.419	1.012	0.661	0.510	0.397	0.251	0.300
367	1.719	1.291	0.931	0.646	0.542	0.468	0.323	0.361
B) ATM Elevation	136	137	138	139	140	141	142	143
364	1.928	1.752	1.546	1.205	0.869	0.594	0.453	0.485
365	1.880	1.665	1.328	0.951	0.701	0.525	0.438	0.412
366	1.857	1.559	1.140	0.806	0.664	0.570	0.382	0.484
367	1.893	1.388	1.087	0.833	0.716	0.638	0.470	0.457
C) Altimeter SD	136	137	138	139	140	141	142	143
364	11.855	8.813	10.973	13.407	16.456	13.988	14.683	18.442
365	10.685	11.256	11.883	10.115	13.502	16.417	15.712	17.179
366	13.805	14.020	12.791	14.524	15.373	17.243	13.119	18.391
367	17.415	9.721	15.519	18.641	17.456	17.057	14.688	9.612
D) PSR SD	136	137	138	139	140	141	142	143
364	43.2	47.6	29.8	36.0	30.6	20.7	19.6	24.6
365	39.7	40.4	34.7	34.9	26.3	18.7	24.8	28.3
366	27.4	27.5	24.3	23.0	22.2	24.1	22.3	23.0
367	20.2	20.2	21.5	23.7	23.3	28.5	22.5	14.8
E) ATM Roughness	136	137	138	139	140	141	142	143
364	15.92	13.29	17.69	21.19	25.59	22.48	23.79	26.51
365	15.02	14.30	15.62	16.63	22.48	23.91	24.50	23.49
366	19.41	19.45	19.56	22.10	24.14	24.90	20.54	26.62
367	25.60	17.73	23.13	27.23	26.19	23.90	22.37	19.21
F) AMSR-E SD	136	137	138	139	140	141	142	143
364	36.44	39.02	30.32	33.32	28.04	22.69	22.73	24.27
365	35.77	36.00	32.60	30.55	26.24	22.66	24.57	25.83
366	28.08	26.00	24.67	24.57	23.19	22.96	23.97	20.45
367	19.25	22.56	21.61	20.87	21.08	22.33	18.57	15.11

depths shows that there is a positive correlation between snow depth and surface roughness for both the altimeter and PSR distributions. This is consistent with previous studies (e.g., [17]). The AMSR-E snow depths are only weakly correlated with the surface roughness and the altimeter and psr snow depths. The latter result is probably due to the spatial sampling difference between aircraft and spacecraft.

In Table III, for the Kotzebue Sound area, both the D2P and ATM elevations show a similar pattern with an increase in elevation from right to left which probably corresponds to a changing geoid. The change is about 1.5 m over a distance of 100 km, length of the P-3 flight line (eight 12.5-km AMSR-E grid cells). A comparison of the altimeter and PSR snow depths shows no agreement for this particular day. In fact, there is deeper snow derived from the altimeters on the right side of the flight area, whereas the PSR deep snow is found on the left side of the area. One possible explanation is that the greatest effects from the mid-February melt/freeze event and storm passages were felt in the upper left of the flight area (see Fig. 9). Because of this large-scale event, the sea ice snow cover in the upper left portion of the flight area may have had ice layers imbedded in the snow cover, which would have been particularly likely if rainfall had occurred. These ice layers may have resulted in lower altimeter snow depths (Table III). Larger size snow grains in the affected area would have also caused the PSR snow depths to be overestimated [18], because of greater scattering at 37 GHz relative to 19 GHz. Unfortunately, we do not have in-situ measurements to confirm this interpretation.

Another factor influencing the altimeter snow depth retrievals is the change in velocity of electromagnetic radiation from air to snow. The snow depth correction (v/c), where v is the wave velocity in snow, c the speed of light in vacuo, is proportional to $\sqrt{(\varepsilon')}$, where ε' is the dielectric permittivity of saline snow (i.e., the real part of the dielectric constant). A dielectric mixture model for saline snow [19] has been used to compute ε'. The model parameterization is a function of snow properties (density ρ, salinity S, and temperature T), and the frequency of the radiation (15 GHz in our case). Our v/c correction ranges between 0.7 ($\rho = 400$ kg/m3 $S = 15$ ppt $T = 265$ K) and 0.8 ($\rho = 300$ kg/m3 $S = 0$ ppt $T = 255$ K). This range has been used to establish uncertainties of the altimeter snow depths (Fig. 12).

We plot the PSR snow depths versus the altimeter snow depths in Fig. 12 for the Chukchi Sea flight on March 21 where we have a total of 880 coincident altimeter and PSR measurements spanning portions of 31 AMSR-E pixels. For the purpose of gaining insight into the effects of the air/snow velocity differences on the snow depth retrievals, we show three regression lines, one for the uncorrected altimeter snow depths (dashed line) and two others for the corrected altimeter snow depths (using the 0.8 and 0.7 v/c factors). The uncorrected velocity has the smallest slope of 0.43, whereas the 0.7 and 0.8 corrected retrievals have slopes of 0.54 and 0.62, respectively. Although these corrections increase the slope slightly, we still have slopes much less than 1. The length of the error bar for each point shown in Fig. 12 is determined from the 0.7 and 0.8 v/c corrections and provides a sense of how much the correction affects the snow depth retrieval. The variation in v/c which depends on the snow properties certainly contributes to the observed scatter. We also indicate surface roughness, which is computed from ATM measurements, for each data point in Fig. 12 through the use of a color scale. It is apparent that both the PSR and altimeter snow depths increase with increasing surface roughness. The correlations between the PSR and altimeter snow depths and surface roughness are 0.60 and 0.67, respectively.

Finally, we calculate comparison statistics based on the PSR and altimeter snow depth data sets for the Chukchi Sea flight on March 21. We have not corrected the altimeter snow depths for air/snow velocity changes, because of the large uncertainty in the snow parameters needed for the correction. These statistics are presented in Table IV. The mean snow depth difference (PSR minus altimeter) is -2.4 cm with a standard deviation of 7.7 cm. The RMS error is 8.0 cm, and the overall correlation between the two snow depth data sets is 0.59.

IV. Summary and Conclusions

Although the original intent of the Arctic 2006 field campaign was to use the airborne altimeters as a validation tool to assess the AMSR-E snow on sea ice retrievals, we could not undertake a validation study, because the altimeter elevation differences as a measure of snow depth on sea ice have yet to be validated. Thus, we could not justifiably use the altimeter snow depths as a validation data set. Nonetheless, a comparison between the altimeter-derived and radiometer-derived snow depths provided insight into the limitations of both approaches.

Of the three flights made over the ice-covered seas surrounding Alaska, only the Chukchi Sea flight made on March 21 provided data which yielded a good correlation between the altimeter and radiometer snow depths. However, the slope of the regression line is much less ($\sim$0.5) than 1. An understanding of this requires a careful comparison of both the altimetric and radiometric retrieval methods with in-situ snow depth measurements. Snow depth retrievals over Kotzebue Sound on March 22 were apparently affected by a melt-freeze event in the previous month. This event may have produced ice layers in the snow cover resulting in an underestimate of snow depth by the altimeters. The first two flights were over first-year ice, whereas the third flight over the Beaufort Sea on March 25 covered an area comprised mostly of multiyear ice. The presence of multiyear ice results in an ambiguous radiometric snow depth signature, because of scattering of the upwelling radiation by empty brine pockets in the freeboard layer of the multiyear ice [20]. It is this ambiguous signature that probably led to the poor correlation between the two snow depth data sets. Currently, there is no way to distinguish between first-year ice with a deep snow cover and multiyear ice.

The potential to retrieve snow depth from airborne lidar and radar altimeter measurements has been demonstrated in several studies (e.g., [12], [14]), but a true validation of this method has not yet been demonstrated. Furthermore, there is a recurrent need to apply an adjustment to the radar altimeter data. Indeed, over some areas, the surface (i.e., the air/snow interface) elevation tracked by the lidar is lower than the snow/ice interface that should be detected by the radar, resulting

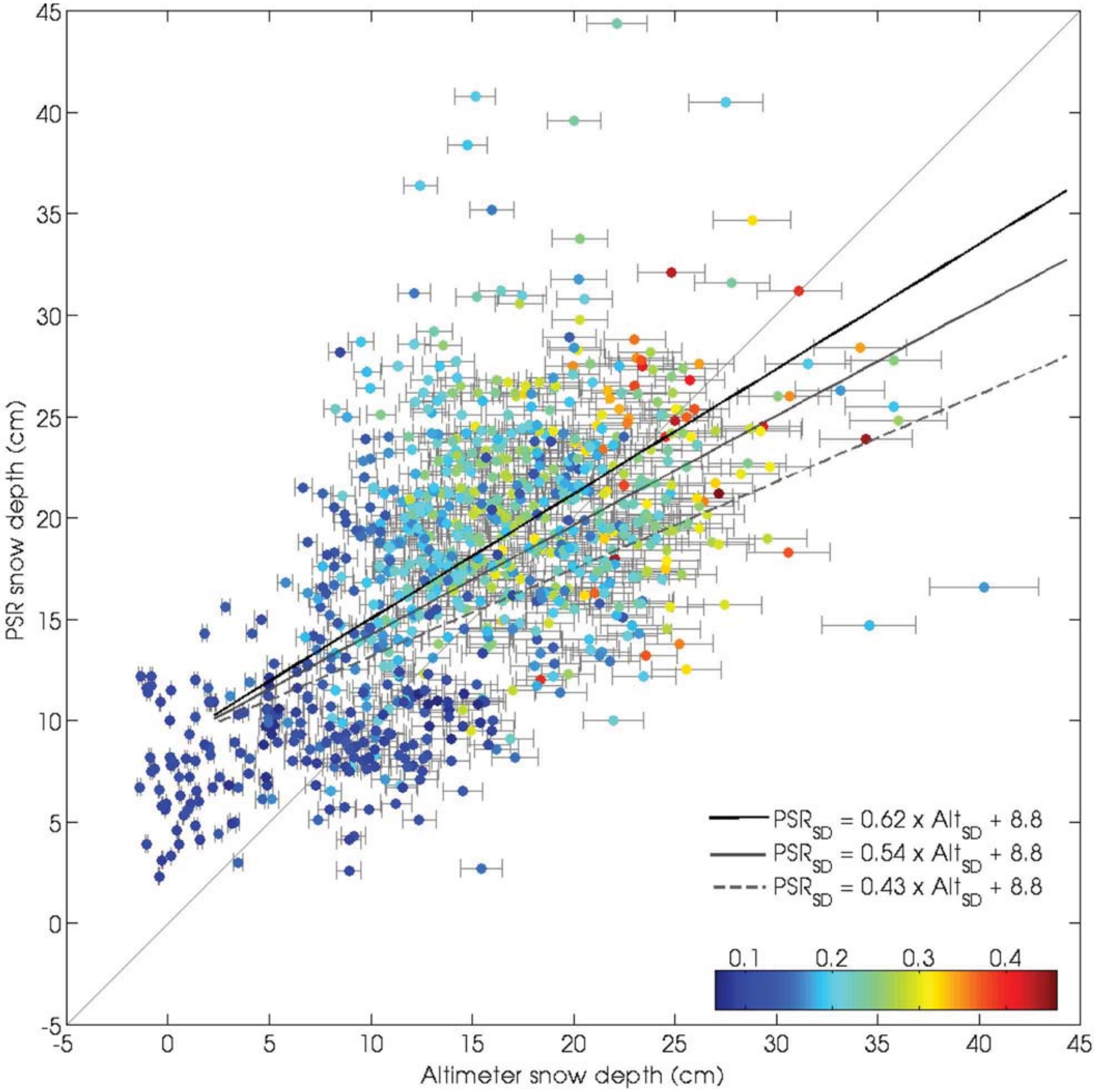

4/C

Fig. 12. PSR snow depths versus the airborne altimeter-derived snow depths for March 21, 2006. There are three regression lines: one for the uncorrected altimeter snow depths (dashed line), one each for the 0.7 v/c corrected (light solid line), and the 0.8 v/c corrected (dark solid line) altimeter snow depths. ATM-derived surface roughness for each point is color coded.

TABLE IV
COMPARISON SNOW DEPTH STATISTICS FOR THE MARCH 21, 2006 CHUKCHI SEA STUDY AREA

Snow Depth Data Set	Snow Depth Range (cm)	Mean Snow Depth ± 1 Stan. Dev. (cm)	Mean Diff. (PSR-Alt SD) ± 1 Stan. Dev. (cm)	RMS Diff. (cm)
PSR (Equiv. AMSR-E)	11.9 – 44.4	17.3 ± 6.9	-2.4 ± 7.7	8.0
Altimeter (ATM-D2P)	1.9 – 53.7	19.7 ± 9.3		

in unrealistic negative snow depths. An explanation of these negative snow depths is problematic. The current study and several previous ones [12], [14], [21] have encountered the need to adjust the radar altimeter measurements relative to the lidar measurements. Understanding this recurrent discrepancy must be a priority for future studies that aim at using the difference between airborne lidar and radar altimeter measurements as a proxy for snow depth.

Finally, the current status of the AMSR-E snow depth algorithm validation is that it is incomplete. We cannot provide an overall estimate of accuracy with any confidence. Some validation studies have been undertaken with in-situ and ship-borne measurements [8], [17], but comparisons between satellite retrievals and surface point measurements can in itself introduce biases [6]. Thus, there is still a critical need to develop validated methods of retrieving snow depth from airborne sensors to help bridge the spatial divide between satellite observations and surface point measurements. Furthermore, the AMSR-E snow depth algorithm currently does not take into account surface roughness or snow grain size variations, even though both of these parameters affect snow depth retrievals [8], [17]. More comparative studies are needed covering different surface conditions at different times of the year. Previous studies [8], [18], [22] suggest that the use of the 10-GHz AMSR-E channels may help both in differentiating between smooth and rough surfaces and in lessening the affect of increasing snow grain size. Thus, work remains to be done to improve snow depth on sea ice retrievals from both microwave radiometers and altimeters.

Acknowledgment

The authors thank the NASA EOS Project Office and the NASA Cryospheric Sciences Program for their full support and the NASA P-3B pilots and their crew for meeting all flight objectives, all of which led to the successful completion of the Arctic 2006 field campaign. We also think the two anonymous reviewers whose comments and recommendations have resulted in a significantly improved manuscript.

We acknowledge both the National Space Science and Technology Center in Huntsville, AL and the National Snow and Ice Data Center in Boulder, Colorado for processing and providing the AMSR-E snow depth on sea ice products. The ECMWF data used in this study are from the Research Data Archive (RDA) which is maintained by the Computational and Information Systems Laboratory at the National Center for Atmospheric Research which is sponsored by the National Science Foundation. The original data (data set number ds627.0) are available from the RDA (http://dss.ucar.edu). The AMSR-E sea ice drift gridded products were obtained from the Centre de Recherche et d'Exploitation Satellitaire (CERSAT), at IFREMER, Plouzané, France (http://cersat.ifremer.fr/data/discovery/by_product_type/gridded_products).

References

[1] D. J. Cavalieri and T. Markus, "EOS aqua AMSR-E Arctic sea ice validation program: Arctic2003 Aircraft campaign flight report," NASA, Greenbelt, MD, NASA TM-2006-214142, p. p. 27, 2006.

[2] N. T. Kurtz, T. Markus, D. J. Cavalieri, W. B. Krabill, J. G. Sonntag, and J. Miller, "Comparison of ICESat data with airborne laser altimeter measurements over Arctic sea ice," *IEEE Trans. Geosci. Remote Sens.*, vol. 46, no. 7, pp. 1913–1924, Jul. 2008.

[3] L. N. Connor, S. W. Laxon, A. L. Ridout, W. B. Krabill, and D. C. McAdoo, "Comparison of Envisat radar and airborne laser altimeter measurements over Arctic sea ice," *Remote Sens. Environ.*, vol. 113, no. 3, pp. 563–570, 2009.

[4] N. T. Kurtz, T. Markus, D. J. Cavalieri, L. C. Sparling, W. B. Krabill, A. J. Gasiewski, and J. G. Sonntag, "Estimation of sea ice thickness distributions through the combination of snow depth and satellite laser altimetry data," *J. Geophys. Res.*, vol. 114, p. C10007, 2009.

[5] T. Kawanishi, T. Sezai, Y. Ito, K. Imaoka, T. Takeshima, Y. Ishido, A. Shibata, M. Miura, H. Inahata, and R. W. Spencer, "The Advanced Microwave Scanning Radiometer for the Earth Observing System (AMSR-E), NASDA's contribution to the EOS for global energy and water cycle studies," *IEEE Trans. Geosci. Remote Sens.*, vol. 41, no. 2, pp. 184–194, Feb. 2003.

[6] T. Markus and D. J. Cavalieri, "Snow depth distribution over sea ice in the Southern Ocean from satellite passive microwave data," in *Antarctic Sea Ice: Physical Processes, Interactions and Variability*, vol. 74. Washington, DC: Amer. Geophys. Union, 1998, ser. Antarctic Research Series, pp. 19–39.

[7] T. Markus and D. J. Cavalieri, "An enhancement of the NASA Team sea ice algorithm," *IEEE Trans. Geosci. Remote Sens.*, vol. 38, no. 3, pp. 1387–1398, May 2000.

[8] T. Markus, D. J. Cavalieri, A. J. Gasiewski, M. Klein, J. A. Maslanik, D. C. Powell, B. Stankov, J. C. Stroeve, and M. Sturm, "Microwave signatures of snow on sea ice: Observations," *IEEE Trans. Geosci. Remote Sens.*, vol. 44, no. 11, pp. 3081–3090, Nov. 2006.

[9] D. T. Eppler, M. R. Anderson, D. J. Cavalieri, J. C. Comiso, L. D. Farmer, C. Garrity, P. Gloersen, T. C. Grenfell, M. Hallikainen, A. W. Lohanick, J. A. Maslanik, C. Matzler, R. A. Melloh, I. Rubinstein, and C. T. Swift, "Passive microwave signatures," in *Microwave Remote Sensing of Sea Ice*, vol. 68, *American Geophysical Union Monograph*, F. D. Carsey, Ed. Washington, DC: Amer. Geophys. Union, 1992, ch. 4, pp. 47–71.

[10] B. Csatho, T. Schenk, W. Krabill, T. Wilson, W. Lyons, G. McKenzie, C. Hallam, S. Manizade, and T. Paulsen, "Airborne laser scanning for high-resolution mapping of Antarctica," *EOS Trans.*, vol. 86, no. 25, pp. 237–238, Jun. 21, 2005.

[11] W. B. Krabill, R. H. Thomas, C. F. Martin, R. N. Swift, and E. B. Frederick, "Accuracy of airborne laser altimetry over the Greenland ice sheet," *Int. J. Remote Sens.*, vol. 16, no. 7, pp. 1211–1222, 1995.

[12] C. J. Leuschen, R. N. Swift, J. C. Comiso, R. K. Raney, R. D. Chapman, W. B. Krabill, and J. G. Sonntag, "Combination of laser and radar altimeter height measurements to estimate snow depth during the 2004 Antarctic AMSR-E Sea Ice field campaign," *J. Geophys. Res.*, vol. 113, p. C04S90, 2008.

[13] W. B. Krabill, W. Abdalati, E. B. Frederick, S. S. Manizade, C. F. Martin, J. G. Sonntag, R. N. Swift, R. H. Thomas, and J. G. Yungel, "Aircraft laser altimetry measurement of elevation changes of the Greenland ice sheet: Technique and accuracy assessment," *J. Geodyn.*, vol. 34, no. 3/4, pp. 357–376, Oct./Nov. 2002.

[14] K. A. Giles, S. W. Laxon, D. J. Wingham, D. W. Wallis, W. B. Krabill, C. J. Leuschen, D. McAdoo, S. S. Manizade, and R. K. Raney, "Combined airborne laser and radar altimeter measurements over the Fram Strait in May 2002," *Remote Sens. Environ.*, vol. 111, no. 2/3, pp. 182–194, Nov. 2007.

[15] D. J. Cavalieri, "A microwave technique for mapping thin sea ice," *J. Geophys. Res.*, vol. 99, pp. 12 561–12 572, 1994.

[16] D. P. Dee, S. M. Uppala, A. J. Simmons, P. Berrisford, P. Poli, S. Kobayashi, U. Andrae, M. A. Balmaseda, G. Balsamo, P. Bauer, P. Bechtold, A. C. M. Beljaars, L. van de Berg, J. Bidlot, N. Bormann, C. Delsol, R. Dragani, M. Fuentes, A. J. Geer, L. Haimberger, S. B. Healy, H. Hersbach, E. V. Hólm, L. Isaksen, P. Kållberg, M. Köhler, M. Matricardi, A. P. McNally, B. M. Monge-Sanz, J. J. Morcrette, B. K. Park, C. Peubey, P. de Rosnay, C. Tavolato, J. N. Thépaut, and F. Vitart, "The ERA-interim reanalysis: Configuration and performance of the data assimilation system," *Q. J. R. Meteorol. Soc.*, vol. 137, no. 656, pp. 553–597, Apr. 2011.

[17] T. Markus, R. Massom, A. Worby, V. Lytle, N. Kurtz, and T. Maksym, "Freeboard, snow depth and sea-ice roughness in East Antarctica from in situ and multiple satellite data," *Ann. Glaciol.*, vol. 52, no. 57, pp. 242–248, 2011.

[18] T. Markus, D. C. Powell, and J. R. Wang, "Sensitivity of passive microwave snow depth retrievals to weather effects and snow evolution," *IEEE Trans. Geosci. Remote Sens.*, vol. 44, no. 1, pp. 68–77, Jan. 2006.

[19] M. Hallikainen and D. Winebrenner, "The physical basis for sea ice remote sensing," in *Microwave Remote Sensing of Sea Ice*, vol. 68, *Geophysical Monograph*, F. Carsey, Ed. Washington, DC: Amer. Geophys. Union, 1992, ch. 3, pp. 29–46.

[20] P. Gloersen, W. Nordberg, T. J. Schmugge, T. T. Wilheit, and W. J. Campbell, "Microwave signatures of first-year and multiyear sea ice," *J. Geophys Res.*, vol. 78, no. 18, pp. 3564–3572, Jun. 1973.

[21] C. Leuschen and R. K. Raney, "Initial results of data collected by the APL D2P radar altimeter over land and sea ice," *Johns Hopkins APL Tech. Dig.*, vol. 26, no. 2, pp. 114–122, 2005.

[22] J. C. Stroeve, T. Markus, J. A. Maslanik, D. J. Cavalieri, A. J. Gasiewski, J. F. Heinrichs, J. Holmgren, D. K. Perovich, and M. Sturm, "Impact of surface roughness on AMSR-E sea ice products," *IEEE Trans. Geosci. Remote Sens.*, vol. 44, no. 11, pp. 3103–3117, Nov. 2006.

Donald J. Cavalieri received the B.S. degree in physics from the City College of New York, New York, in 1964, the M.A. degree in physics from Queens College, New York, in 1967, and the Ph.D. degree in meteorology and oceanography from New York University, New York, in 1974.

From 1974 to 1976, he was a National Research Council Postdoctoral Resident Research Associate with the National Oceanic and Atmospheric Administration Environmental Data Service, Boulder, CO, where he continued his doctoral research on stratospheric-ionospheric coupling. In 1979, he joined the Laboratory for Atmospheres, National Aeronautics and Space Administration (NASA) Goddard Space Flight Center, Greenbelt, MD. In 2009, after 30 years working on sea ice algorithm development and validation for satellite microwave radiometers and on cryospheric system science, he retired as a NASA Senior Research Scientist with the Cryospheric Sciences Branch, Hydrospheric and Biospheric Sciences Laboratory. He continues to work as a part-time consultant within the Cryospheric Sciences Laboratory. His current research activities center on the refinement and validation of sea ice algorithms for the Advanced Microwave Scanning Radiometer for EOS and the development of sea ice climate data records.

Thorsten Markus received the M.S. and Ph.D. degrees in physics from the University of Bremen, Bremen, Germany, in 1992 and 1995, respectively.

He is currently the Head of the Cryospheric Sciences Branch, Hydrospheric and Biospheric Sciences Laboratory, Goddard Space Flight Center, National Aeronautics and Space Administration, Greenbelt, MD. His research interests include satellite and airborne remote sensing of cryospheric, oceanic, and atmospheric processes. He is the Project Scientist for ICESat-2.

Alvaro Ivanoff received the B.Sc. degree in physics from the University of Toronto, Toronto, ON, Canada, in 1997.

He is currently working at NASA Goddard Space Flight Center, Greenbelt, MD, through ADNET Systems, Inc. supporting algorithm development and validation.

Jeff A. Miller received the B.S. degree in physics from the University of Maryland, College Park, in 1994.

He is currently with Wyle Inc., supporting algorithm development and calibration in the Cryospheric Sciences Lab at National Aeronautics and Space Administration Goddard Space Flight Center (GSFC), Greenbelt, MD. From 1998 to 2004, he supported the Landsat Project Science Office at GSFC. His research interests are in radiometry (microwave and reflective), new data products and improving product quality.

Ludovic Brucker received the M.S. degree in physics from the University of Clermont-Ferrand, France, in 2006 and the Ph.D. degree from the Laboratoire de Glaciologie et Geophysique de l'Environnement, Grenoble University/Centre National de la Recherche Scientifique, Grenoble, France, in October 2009.

He joined National Aeronautics and Space Administration Goddard Space Flight Center/GESTAR, Greenbelt, MD, in 2010. His research focuses on understanding the passive microwave emission of snow-covered polar and subpolar regions (i.e., over sea ice, ice sheet, and land) to derive climate-related variable. The goal of his work is to contribute to the comprehension of the relationships between both passive and active microwave space-borne observations and snow physical properties using modeling approaches. He has also participated in the International Polar Year in 2008 with a deployment to North Quebec and has been deployed on the West Antarctic Ice Sheet in 2011.

M. Sturm, photograph and biography not available at the time of publication.

James A. Maslanik received the Ph.D. degree in geography from the University of Colorado, Boulder, in 1984, and the Masters of Environmental Pollution Control degree and the Bachelor of Science degree in forest science from the Pennsylvania State University, University Park, in 1980 and 1978, respectively.

He is a Research Professor in the Department of Aerospace Engineering Sciences at the University of Colorado, Boulder. His research interests include polar climatology, the interactions of sea ice with atmosphere and ocean, remote sensing and field investigations of sea ice properties, and development and deployment of unpiloted aerial vehicles for polar research.

John F. Heinrichs received the B.S. degree in mathematics and the M.S. degree in mathematics from the University of Wisconsin-Milwaukee, Milwaukee, in 1983 and 1985, respectively, and the Ph.D. degree in geography from the University of Colorado at Boulder, Boulder in 1996.

He worked as a Staff Scientist at Hughes Aircraft Company, Culver City, CA, from 1986 until 1992, as a Research Assistant at the Cooperative Institute for Research in Environmental Sciences (CIRES), Boulder, from 1992 until 1996, as a Postdoctoral Researcher at CIRES, from 1996 until 1998, and has been on the faculty at Fort Hays State University, Hays, KS, where he currently serves as Professor and Chair of the Department of Geosciences, since 1998.

Dr. Heinrichs is a member of the IEEE Geoscience and Remote Sensing Society, the American Geophysical Union, and the Association of American Geographers.

Albin J. Gasiewski (SM'81–M'88–SM'95–F'02) received the M.S. and B.S. degrees in electrical engineering and the B.S. degree in mathematics from Case Western Reserve University, Cleveland, OH, in 1983, and the Ph.D. degree in electrical engineering and computer science from the Massachusetts Institute of Technology, Cambridge, in 1989.

From 1989 to 1997, he was a Faculty Member with the School of Electrical and Computer Engineering, Georgia Institute of Technology, Atlanta, where he became an Associate Professor. He has developed and taught courses on electromagnetics, remote sensing, instrumentation, and wave propagation theory. From 1997 to 2005, he was with the U.S. National Oceanic and Atmospheric Administration's Environmental Technology Laboratory (ETL), Boulder, CO, where he was Chief of ETL's Microwave Systems Development Division. He is currently a Professor of electrical and computer engineering with the University of Colorado at Boulder (CU-Boulder) and Director of the CU-Boulder Center for Environmental Technology. His technical interests include passive and active remote sensing, radiative transfer, antennas and microwave circuits, electronic instrumentation, meteorology, and oceanography.

Dr. Gasiewski is past President (2004-2005) of the IEEE Geoscience and Remote Sensing Society (GRSS). He is a member of the American Meteorological Society, the American Geophysical Union, the International Union of Radio Scientists (URSI), Tau Beta Pi, and Sigma Xi. He currently serves as Vice Chair of U.S. National Committee/URSI Commission F. He served on the U.S. National Research Council's Committee on Radio Frequencies from 1989 to 1995. He was the General Cochair of the 2006 International Geoscience and Remote Sensing Symposium, Denver, CO, and a recipient of the 2006 Outstanding Service Award from the GRSS.

C. Leuschen received the B.S. and M.S. degrees in electrical engineering from The University of Kansas, Lawrence, in 1995 and 1997, respectively.

Since 1995, he has been with the Radar Systems and Remote Sensing Laboratory, University of Kansas, where he was a Graduate Teaching Assistant for the Sensor Design Laboratory. His research interests include ground-penetrating radar, numerical electromagnetics, and signal processing with emphasis on wave migration and synthetic aperture radar.

William Krabill received the B.S. in mathematics from Salisbury University, Salisbury, MD, in 1968.

He joined NASA at Wallops Island, VA, in 1968 as a Mathematician and Data Analyst for the radar systems section. He was the Project Manager and Principal Investigator for airborne lidar topographic mapping and Global Positioning System applications in the Cryospheric Sciences Branch at the Goddard Space Flight Center/Wallops Flight Facility. By the year 2000, the project had collected more than 4 000 000 000 surface elevation measurements over extensive portions of the Greenland Ice Sheet—65 000 kilometers of track line in 1998 and 1999 alone. He has been the PI and Team Leader from 1991 to 2008, when he retired to part-time activities. He continues to be active in the management of the project and assists in directing the planning, execution, and subsequent data processing and analysis.

Mr. Krabill is a member of the American Geophysical Union.

J. Sonntag, photograph and biography not available at the time of publication.

AUTHOR QUERIES

AUTHOR PLEASE ANSWER ALL QUERIES

Please be aware that authors are required to pay overlength page charges ($200 per page) if the paper is longer than 6 pages. If you cannot pay any or all of these charges please let us know.

AQ1 = Please provide keywords.
AQ2 = Please expand "EOS."
AQ3 = Please expand "GESTAR."

END OF ALL QUERIES